

# Dynamics of deformable air bubbles rising in water

K Haase<sup>1\*</sup>, J Haßberger<sup>2</sup>, M Klein<sup>2</sup> and CJ Kähler<sup>1</sup>

<sup>1</sup> Universität der Bundeswehr München, Institute of Fluid Mechanics and Aerodynamics, München, Germany

<sup>2</sup> Universität der Bundeswehr München, Institute of Mathematics and Applied Computing, München, Germany

\* katharina.haase@unibw.de

## Abstract

Experimental and numerical analyses were performed to resolve the complex 3D deformation and periodic shape oscillations of deformable air bubbles in water (~ 4–5 mm diameter). Characterizing the temporal variation of the surface-to-volume ratio was the primary interest of this investigation. It is shown that the surface-to-volume ratio oscillates with two dominant frequencies (or modes) called  $f_R$  and  $f_S$  modes in the following. In the literature, the oscillation modes are derived from 2D data by evaluating the temporal variation of the elliptical axes of the deformed bubbles. Significant differences can be detected between the literature values and our 3D data, suggesting that, for bigger bubbles, a 3D evaluation becomes necessary to avoid bias errors.

## 1 Introduction

Gas bubbles are frequently used in industry for two reasons. First, bubbles transfer gaseous chemicals into a liquid medium so that the desired chemical reactions can take place. Second, they enhance the mixing by generating turbulence. Mixing is very important for chemical reactions, as molecules of different species must come into contact for the reaction to occur. In most technical applications, bubbles of diameter 1–10 mm are used with up to 10% volume fraction. The transfer of chemicals from the bubbles into the liquid depends strongly on the flow state of the surrounding media (laminar/turbulent). The size of the bubble is also an important parameter, since larger bubbles deform in a complex manner (Clift 1978). This results in a variation of the surface area, which can have an effect on the transfer of chemicals through the interface. The wake structure of the bubbles, and thus the generated turbulence level, depends on the size, shape and oscillatory modes of the bubbles. In order to understand how the mass transfer depends on the flow state and the bubble deformation, it is necessary to investigate the details of the 3D bubble dynamics in a turbulent flow.

The specific aim of this work is to experimentally and numerically determine and characterize the shape oscillations of large bubbles. Several previous works have been published about the studies of freely rising bubbles, such as Lamb (1932), Tsamopoulos (1983) and Wang (1996). However, those examinations mainly focus on small bubbles. In this case, the deformations are of small amplitude and the oscillations can be described in terms of spherical harmonics. If larger bubbles are considered, the amplitude of the oscillations lead to non-linear effects, as the inviscid frequency shift described by Tsamopoulos (1983), for instance. Hartunian and Sears (1957) studied large scale lateral motion of bubbles, following mainly zig-zagging and spiraling paths, and suggested that an interaction between capillary shape oscillations and the translation of the bubble is responsible for the behavior. Meiron (1989), on the other hand, did not find such interaction in his numerical results.

It is evident that the shape of a bubble fluctuates as a result of the turbulent shear and pressure forces of the surrounding liquid. In addition to that, the coupled vortex shedding behind rising bubbles leads to

lateral motion of the bubbles, inducing drag and lift forces on the bubbles. This was also observed by Fan and Tsuchiya (1990), who reported a shape oscillation with a frequency of the lateral motion. To describe these oscillations in the literature, two different modes are discussed: the oscillations in the equivalent major axis, named mode 2,0; and of that in the axes ratio, as mode 2,2.

In Lunde and Perkinson (1997), a simple model is described linking the shape oscillations to capillary waves travelling on the bubble surface. Meiron (1989) noted that bubble shape oscillations have the character of progressive waves. The 2,0 waves are moving from the front to the rear stagnation points (from pole the pole), and mode 2,2 waves are travelling around the equator of the bubbles. In Fig. 1 a sketch visualizing the two modes is shown. It is further described in Lunde and Perkinson (1997) that the modes correlate with the bubble volume and deformation. The frequencies of the oscillations can be formulated in terms of the spherical equivalent diameter  $2r_\epsilon$  and the ellipticity  $\epsilon$ . The speed of the capillary wave  $C$  can be calculated by  $C = \sqrt{2\pi\sigma / \lambda_n \rho_L}$ . In this formula,  $\lambda_n$  denotes the wavelength, with the mode  $n$  around the bubble circumference,  $\sigma$  the surface tension, and  $\rho_L$  the density of the liquid. The mode 2,0 and 2,2 frequencies can be calculated according to Lunde and Perkinson (1997) as follows:

$$f_{2,0} = \frac{1}{2\pi} \sqrt{\frac{16\sqrt{2}\epsilon^2\sigma}{\rho_L(\epsilon^2+1)^{\frac{3}{2}}r_\epsilon^3}} \quad \text{and} \quad f_{2,2} = \frac{1}{2\pi} \sqrt{\frac{8\sigma}{\rho_L\epsilon r_\epsilon^3}} \quad (1)$$

The oscillation frequencies for small bubbles with a diameter up to 2–3 mm are well reported in the literature, but the deformation dynamics of larger bubbles is less well documented, see Lunde and Perkinson (1997) or de Vries (2002). Bubbles with a larger diameter become unstable and start to deform in such a manner that it is more difficult to measure or simulate their dynamics and surface motion. The aim of this work is to analyze the deformation dynamics of larger bubble with a diameter between 4–5 mm by using a novel 3D-reconstruction technique and direct numerical flow simulation. Thanks to the 3D analysis approach, it becomes possible to analyze the surface-to-volume ratio of the bubbles. The surface-to-volume ratio covers 3D effects and is in particular relevant for the estimation of the mass transfer from the bubble into the liquid medium. It will be shown that the surface-to-volume ratio is a good measure to detect and characterize periodic bubble deformations.

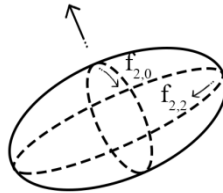


Figure 1 Sketch to visualize the mode 2,0 and 2,2 waves. The 2,0 waves are moving from the front to the rear stagnation points (from pole the pole), and mode 2,2 waves are travelling around the equator of the bubbles.

## 2 Experimental Setup

The experiments were conducted in the countercurrent channel (see Fig. 2) at the Universität der Bundeswehr in Munich. Four LaVision Imager Pro HS cameras were used to record data at up to 0.6 kHz. In order to better recognize and evaluate the bubble, LED backlights were installed on the opposite side of the cameras. The commercial software DaVis from LaVision was used for the recording. Since the bubbles can move freely over the whole channel, a large measurement volume is desired. However, as a good reconstruction result requires a high spatial resolution, the volume has to be rather small to resolve

small amplitudes of the shape oscillations. Thus, a compromise was found with a  $20 \times 20 \times 20 \text{ mm}^3$  volume. The measurement volume was located in the middle of the channel to avoid wall interactions and boundary layer effects.

To keep the bubble in this measurement volume for a sufficiently long period of time, the flow speed in the test section was aligned with the raising speed of the bubbles by using an electronic control valve at the lower end of the channel. To ensure a homogeneous inflow with desired turbulent velocity fluctuations, a turbulence generator was installed above the measuring section. The turbulence generator consists of solid particles with a specific size, shape, and volume densities that were arranged in a regular manner by using thin yarn. Thanks to the flexibility of the yarn, the particles can oscillate around their equilibrium location under the action of the flow. In Haase et al. (2017), different types of particle grids were characterized in detail. For the experiments in this paper, a grid with 5 mm ellipses and 10% by volume was used. These grids can be used to create turbulences similar to bubbly swarms in the near field behind the particles. However, to ensure comparability with the numerical results, the measurement volume was placed roughly 50 mm behind the grids. Here the turbulence intensity is slightly lower and more homogeneous, but the statistical properties better match the conditions of the numerical flow simulations.

For the oscillation measurement, 4 mm bubbles are used. The bubbles were created 0.5 m below the measurement volume with appropriate nozzles. The size of the bubbles is highly reproducible. For each measurement, several bubbles were released in the channel with at least 50 bubble diameters between them to avoid wake interactions. As already mentioned, to make a longer recording in the 3D-volume possible and to generate the turbulence with the particle grids, a counterflow was generated such that the velocity of the liquid is comparable with the vertical mean motion of the air bubbles. With a recording frequency of 600 Hz, the recording allows to resolve oscillations up to 300 Hz.



Figure 2 Schematic diagram of the countercurrent channel (left). The flow velocity is regulated by an electric valve at the end of the measuring section. In order to generate a continuous flow, the fluid is pumped back into the water basin. The turbulence generators are located between the measuring section and the nozzle. Schematic representation of the camera setup (right) with controlled background lighting. White LEDs are used as backlight for better contrast in the shadows.

The 3D-surface of the bubble was reconstructed based on the shadow images of four high speed cameras with a MLOS algorithm, as it is implemented in the commercial software DaVis. The MLOS algorithm multiplies the line of sights of each individual camera view to project the surface of the bubble onto the 3D space. With a Matlab-Code, ellipses were fitted to the data to measure the shape and calculate the surface area. In Fig. 3 (left) an example of a reconstructed bubble is shown.

To obtain a comprehensive picture of the complex phenomenon, the extensive experimental study is complemented by Direct Numerical Simulations (DNS), resolving the full spectrum of turbulent scales. This facilitates a direct comparison with experimental data, but also assists the physical interpretation. The

state-of-the-art two-phase flow solver PARIS (PARallel Robust Interface Simulator), described by Ling et al. (2017) and Tryggvason et al. (2011), implements the one-fluid formulation of the unsteady incompressible Navier-Stokes equations including gravitational and capillary forces. Two immiscible fluids are represented by a jump in density and viscosity. Propagation of the phase interface is implicitly calculated by an advection equation for the cell-based volume fraction of one of the phases. Cell-averaged fluid properties are then obtained from an arithmetic mean for density, and a harmonic mean for dynamic viscosity. In terms of in-cell interface treatment, advanced numerical techniques are applied: a geometrical Volume-Of-Fluid method including piece-wise linear interface reconstruction and a height function method combined with continuous surface force balancing for interface curvature determination.

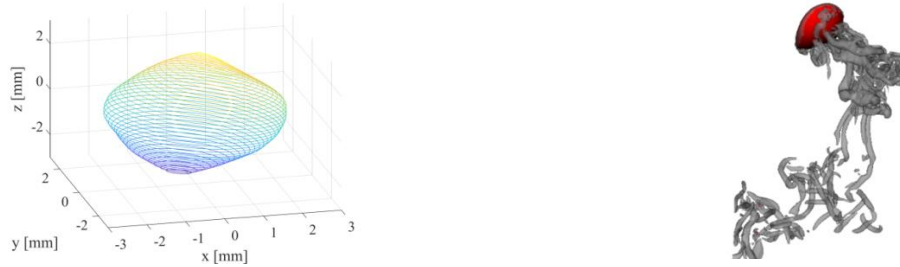


Figure 3 Highly deformable bubble in both experiment (left) and numerical simulation (right). In the simulation the coherent structures in the bubble wake are also visualized by using the Q-criterion.

### 3 Results and Discussion

Since the tomographic measurement technique allows only for a small field of view due to the spatial resolution constraints outlined above, the rising path itself cannot be fully resolved in this experiment. However, at least half of the spiraling motion can be seen in the recorded data. Nevertheless, in this analysis only the deformation is considered and compared with the numerical results from the simulation. According to Lunde and Perkins (1997) it is expected that bubbles with a radius of 4 mm exhibit frequencies in the range of 41 Hz for the  $f_{2,0}$  (oscillation of the major axis) and 28 Hz for the  $f_{2,2}$  (oscillation in the axis ratio). The  $f_{2,2}$  frequency from the shadow images used for the 3D reconstruction was evaluated for comparison. The result is  $f_{2,2} \sim 25$  Hz, which is in acceptable agreement with the literature value taking the differences of the boundary conditions into account. Thanks to the 3D reconstruction and the simulation, it is possible to investigate the surface-to-volume ratio in order to gain a better understanding of the complexity of the 3D deformation.

Figure 4 shows the surface-to-volume ratio calculated from the 3D measurement (left image) and the numerical simulation (center image) for comparison. Two dominant frequencies can be clearly seen in the measured data, called  $f_R$  and  $f_S$ .  $f_R$  describes the frequency of the superimposed oscillation (mean value of the individual frequencies), and  $f_S$  the frequency of the envelope. By considering the specific frequencies of the bubble deformation modes that describe the lateral  $f_{2,0}$  and axial deformation  $f_{2,2}$  oscillations, we can write  $f_R = (f_{2,0} + f_{2,2})/2$  and  $f_S = |f_{2,0} - f_{2,2}|/2$ . A summary of all frequencies for the measured bubble diameters is given in Tab. 1.

The measurement clearly shows that two frequencies dominate the deformation dynamics for 4 mm bubbles: a low one with  $f_S = 13$  Hz, and a high one with  $f_R = 48$  Hz. The high frequency is possibly induced by capillary waves, while the low frequency seems to correlate with the periodic motion of the bubble. The simulation for 5 mm bubbles shows a dominant frequency around 25–30 Hz, which matches nicely the theoretical  $f_R$  value. A dominant frequency of lower value is difficult to estimate from Fig. 4 (center). However, in the right graph the components of the trajectory of the bubble are displayed and it is visible that the bubble performs a zigzag-like motion with a frequency of around 5 Hz. This frequency agrees well with the theoretical  $f_S$  value, but it has to be mentioned that the cause of this oscillation is not

the capillary wave considered in the theory. The problem is that the deformation induced by the capillary wave and the deformation induced by the periodic bubble path (zigzag, or spiral motion) cannot be distinguished from one another.

Another interesting observation is that a correlation exists between the shape deformation due to the capillary waves and the path oscillations. This is indicated by  $R'$  in Fig. 4 (right), which fluctuates with a frequency of around 30 Hz. The high frequency oscillation of  $R'$ , which is superimposed on the low frequency path oscillation of the bubble, is possibly a result of the varying aerodynamic forces on the bubble due to high frequency geometry changes induced by the capillary waves. The analysis shows the potential of the combined experimental and numerical analysis. However, to confirm the physical interpretations, more measurements and simulations are required to resolve the physical interactions in detail.

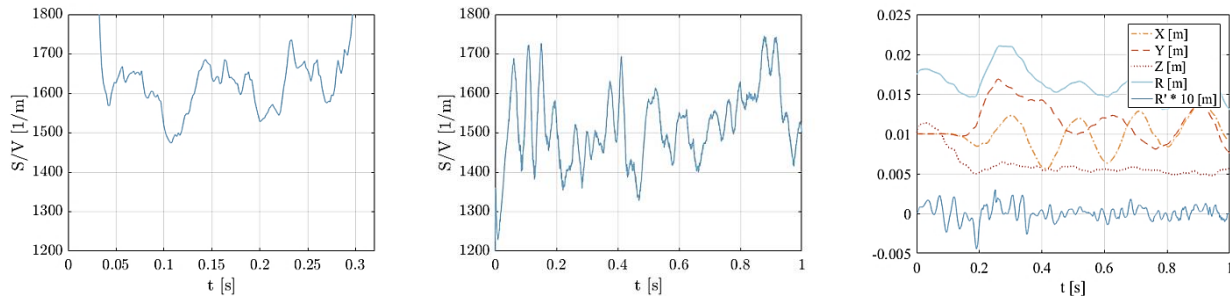


Figure 4 Surface-to-volume ratio measured from the 3D reconstruction (left) and the simulation (center). On the right side the path oscillations of the bubble split in its components derived from the simulations. While  $X$ ,  $Y$ ,  $Z$  are the coordinates bubbles center of mass (right) in space,  $R = \sqrt{X^2 + Y^2 + Z^2}$  and  $R' = R - R_{\text{filtered}}$ .

| $D_{\text{eq}}$ (mm)   | $f_{2,0}$ (Hz) | $f_{2,2}$ (Hz) | $f_R$ (Hz) | $f_S$ (Hz) |
|------------------------|----------------|----------------|------------|------------|
| literature/theoretical |                |                |            |            |
| 4.0                    | 41             | 28             | 34.5       | 6.5        |
| 5.0                    | 29             | 20             | 24.5       | 4.5        |
| experimental           |                |                |            |            |
| 4.0                    | 61             | 35             | 48         | 13         |

Table 1 Comparison of the different frequencies from the reconstruction (exp.), and theoretical calculation taken from literature. For the first literature/theoretical values  $f_R$  and  $f_S$  are calculated from  $f_{2,0}$ ,  $f_{2,2}$  ( $f_{2,0}$ ,  $f_{2,2}$  are calculated with eqn. 1 for the specific diameter). The experimental  $f_{2,0}$  and  $f_{2,2}$  values are calculated from  $f_R$  and  $f_S$  ( $f_R$  and  $f_S$  are derived from the measurement, see Fig. 4 left).

## 4 Conclusions

With the introduced method for a 3D-shape reconstruction and numerical simulations, it was possible to resolve the complex deformation dynamics of bubbles with a diameter of 4 and 5 mm due to capillary waves and aerodynamic forces.

From our experiments and simulations, it is possible to conclude that, for highly deformable bubbles, two dominant frequencies exist ( $f_R$  and  $f_S$ ), which interact with each other in a complex manner. The decomposition of the modes yield two frequencies  $f_{2,0}$  and  $f_{2,2}$ , which can be associated with capillary waves. Moreover, it can be concluded from the numerical results that the capillary waves induce

aerodynamic forces as they alter the shape of the bubble and thus the aerodynamic loads. This in turn alters the bubble path with high frequency. The high frequency path oscillations caused by the capillary waves are superimposed on the low frequency motion (zigzag or spiral) of the bubble.

The analysis shows that the presented 3D approaches are capable of resolving the 3D bubble deformations with high spatial and temporal resolution. The experimental results agree fairly well with direct numerical simulations, taking the different bubble size into account.

In the future, this experimental approach will allow for investigating the complex interaction between the bubble path, the vortex shedding, and the shape oscillation in a turbulent flow field in more detail, so that a deeper understanding of the physical phenomena can be obtained. In combination with the direct numerical simulations, the small details can also be resolved, which are not accessible with experimental techniques, or quantities which cannot be measured.

## Acknowledgements

This project was funded by the DFG as part of the projects SPP1740 KA 1808/18-2 and KL 1456/4-1.

## References

Deckwer WD (1985) Reaktionstechnik in Blasensäulen. *Salle und Sauerländer, Frankfurt am Main*

Fan L-S and Tsuchiya K (1990) Bubble Wake Dynamics in Liquids and Liquid-Solid Suspensions. *Butterworth-Heinemann, Boston*

Haase K, Kück UD, Thöming J and Kähler CJ (2017) On the emulation of bubble induced turbulence by randomly moving particles in a grid structure. *CET* <https://doi.org/10.1002/ceat.201600687>

Lamb H (1932) Hydrodynamics, 6th edition. *Cambridge University Press, Cambridge*

Hartunian, RA and Sears WR (1957) On the stability of small gas bubbles moving uniformly in various liquids. *J. Fluid Mech.* 3, 27–47.

Ling Y, Fuster D, Zaleski S & Tryggvason G (2017) Spray formation in a quasiplanar gas-liquid mixing layer at moderate density ratios: A numerical closeup, *Physical Review Fluids*: 2, 014005.

Lunde K, Perkins RJ (1997) Shape Oscillations of Rising Bubbles. *Flow, Turbulence and Combustion* 58: 387., <https://doi.org/10.1023/A:1000864525753>

Meiron DI (1989) On the stability of gas bubbles in an inviscid fluid. *J. Fluid Mech.*, 198, 101–114.

Tryggvason G, Scardovelli R and Zaleski S (2011) Direct numerical simulations of gas-liquid multiphase flows, *Cambridge University Press, UK*.

Tsamopoulos JA and Brown RA (1983) Non-linear oscillations of inviscid drops and bubbles. *J. Fluid Mech.*, 127 519–537

de Vries AWG, Biesheuvel A, van Wijngaarden L (2002) Notes on the path and wake of a gas bubble rising in pure water. *Int. J. Multiphase Flow*, 28 1823–1835

Wang TG, Anilkumar AV and Lee CP (1996) Oscillations of liquid drops: Results from USML-1experiments in space. *J. Fluid Mech.*, 308 1–14.